Electronic Supplementary Information

Dual Transition-metal Atoms Doping: An Effective Route to Promote the ORR and OER Activity on MoTe$_2$

Can Gao[a], Dewei Rao*[ab], Huan Yang[a], Shaokang Yang[a], Jingjing Ye[a], Shasha Yang[a], Chaonan Zhang[a], Xuecheng Zhou[a], Tianyun Jing[a] and XiaoHong Yan*[a]

[a] Institute for Advanced Materials, School of Materials Science and Engineering, Jiangsu University, Zhenjiang 212013, P. R. China. Email: dewei@ujs.edu.cn; yanxh@ujs.edu.cn
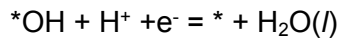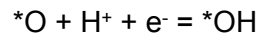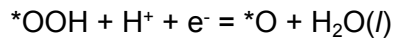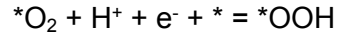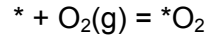
[b] Department of Chemistry and Biochemistry, University of California at Santa Cruz, 1156 High Street, Santa Cruz, California, 95064, United States

Computational details

In this work, all DFT calculations were performed with the Vienna Ab initio Simulation Package (VASP)[1, 2] using the generalized gradient approximation (GGA)[3] and the Perdew-Burke-Eznerhof (PBE)[4] function. The DFT-D3 semi-empirical van der Waals correction was included to deal with dispersion interactions.[5] The spin polarization was considered throughout all the calculations. For geometry optimization, all atomic positions, cell shape and volume were fully relaxed for bulk crystals, while only atomic positions relation was allowed for surface models. The monolayer structure was obtained by cleaving (001) plane of the 2H-MoTe$_2$. Then a 3 × 3 × 1 MoTe$_2$ monolayer supercell with 9 Te and 18 Mo atoms is constructed. A 15 Å vacuum is adopted along c axis to avoid interaction between two adjacent layers due to the periodic boundary condition. The ion-electron interactions were described by the projector augmented wave (PAW)[6] method with the plane-wave kinetic energy cutoff of 500 eV. The Brillouin zone was sampled using the Monkhorst-Pack method[7] with a 3 × 3 × 1 Γ-centered for the structure optimization and a denser 7 × 7 × 1 mesh for obtaining the electronic structures. The convergence criterion for force and total energy were set as 0.015 eV/Å and 10^{-5} eV per atom, respectively. Moreover, the Bader charge analysis was employed to evaluate electronic redistribution before and after adsorption of intermediates. In electrochemistry, the overall ORR/OER pathways on catalyst were calculated in detail according to electrochemical framework developed by Nørskov and his co-workers.[8, 9] As for ORR in acidic electrolyte, the overall reaction process can be summarized as:

$$O_2(g) + 4H^+ + 4e^- = 2H_2O$$
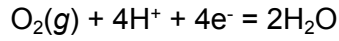
The ORR may proceed through the following elementary steps, which are usually employed to investigate the electrocatalysis of the ORR on various materials:

$$* + O_2(g) = *O_2$$

$$*O_2 + H^+ + e^- + * = *OOH$$

$$*OOH + H^+ + e^- = *O + H_2O(l)$$

$$*O + H^+ + e^- = *OH$$

$$*OH + H^+ + e^- = * + H_2O(l)$$

where * represents an active site on the bare catalysts surface, and $*O_2$, $*OH$, $*O$, $*OOH$ represent four different catalytic intermediates, respectively, g and l refer to the gas and liquid phase.

The reaction free energy (ΔG) for each ORR step above can be related to equation as:

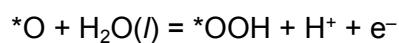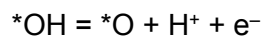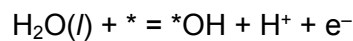$$\Delta G_0 = G_{*O_2} - G_* - 2G_{H_2O}(l) + 2G_{H_2}(g) - 4.92eV$$

$$\Delta G_1 = G_{*OOH} - G_{*O_2} - 1/2G_{H_2}(g)$$

$$\Delta G_2 = G_{*O} - G_{*OOH} - 1/2G_{H_2}(g)$$

$$\Delta G_3 = G_{*OH} - G_{*O} - 1/2G_{H_2}(g)$$

$$\Delta G_4 = G_* + G_{H_2O}(l) - G_{*OH} - 1/2G_{H_2}(g)$$

The mechanism for OER could be written as:

$$H_2O(l) + * = *OH + H^+ + e^-$$

$$*OH = *O + H^+ + e^-$$

$$*O + H_2O(l) = *OOH + H^+ + e^-$$

$$*OOH = O_2(g) + H^+ + e^- + *$$
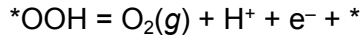
The reaction free energy for each OER step hence was calculated by the following equations:

$$\Delta G_1 = G_{*OH} + 1/2G_{H_2}(g) - G_{H_2O}(l) - G_*$$

$$\Delta G_2 = G_{*O} + 1/2G_{H_2}(g) - G_{*OH}$$

$$\Delta G_3 = G_{*OOH} + 1/2G_{H_2}(g) - G_{*O} - G_{H_2O}(l)$$

$$\Delta G_4 = 4.92eV + 2G_{H_2O}(l) - 2G_{H_2}(g) + 1/2\ G_{H_2}(g) + G_* - G_{*OOH}$$

Considering that the high spin ground state of the O_2 molecule is poorly described in the current DFT scheme, the free energy of the O_2 molecule was derived according to $G_{O_2} = 2\ G_{H_2O}(l) - 2\ G_{H_2}(g) + 4*1.23$ (eV).

The RHE model developed by Nørskov and co-workers[10] was used to obtain the Gibbs reaction free energy of these electrochemical elementary steps. In this model, we set up RHE as the reference electrode, which allows us to replace chemical potential (μ) of the proton–electron pair with that of half a hydrogen molecule: $\mu_{H^+} + \mu_{e^-} = 1/2\mu_{H2}$, at conditions with U= 0 V and P_{H2}= 1 bar.

The free energy change from initial states to final states can be obtained by the following expression:

$$\Delta G = \Delta E + \Delta ZPE - T\Delta S + \Delta G_u + \Delta G_{pH}$$

Here ΔE is the adsorption energies of adsorbed intermediates obtained from DFT ΔE computations. ΔZPE and ΔS are the changes of zero-point energy and the entropic contribution, T is the temperature (298.15K). ΔG_u = -eU, where U is the electrode potential.

$\Delta G_{pH} = k_b T ln10 \cdot pH$, where k_b is the Boltzmann constant and in the present work, pH = 0 was employed. More detailed, the values of ZPE could be derived by the vibrational frequency results, as given:

$$ZPE = 1/2 \sum h v_f$$

Moreover, applying the method proposed by Nørskov et al.,[11] the thermodynamic overpotential η of OER and ORR for a given electrocatalyst was determined by:

$$\eta_{OER} = max\,[\Delta_{G1}, \Delta_{G2}, \Delta_{G3}, \Delta_{G4}]/e - 1.23\ V$$

$$\eta_{ORR} = max\,[\Delta_{G1}, \Delta_{G2}, \Delta_{G3}, \Delta_{G4}]/e + 1.23\ V$$

The binding energy (E_b) of TM atoms doped $MoTe_2$ was calculated as follows:

$$E_b = E_{TM} + E_{sub} - E_{total}$$

where E_{sub} and E_{TM} are the total energy of defective 2D-$MoTe_2$ and TM single atom. E_{total} is the total energy of TM doped $MoTe_2$.

The adsorption energy (E_{ads}) of intermediates was obtained by equation below:

$$E_{ads} = E\,(* + adsorbate) - E\,(*) - E\,(adsorbate)$$

in which E (* + adsorbate), E (*) and E (adsorbate) are the total energy of TM doped $MoTe_2$ with adsorbed intermediates, TM doped $MoTe_2$, and intermediates, respectively.

The formation energy (E_f) of different doping structure was calculated with the following formula:

$$E_f = E_{CoM/MoTe2} + \mu_{Te} - (E_{V-MoTe2} + \mu_{Co} + \mu_M)$$

where $E_{CoM/MoTe2}$ and $E_{V-MoTe2}$ are the total energies of vacancy $MoTe_2$ with and without doping, respectively. μ_{Te}, μ_{Co} and μ_M are the chemical potentials of Te, Co and M (M= Fe, Ni, Cu, Zn, Pd and Pt), respectively.

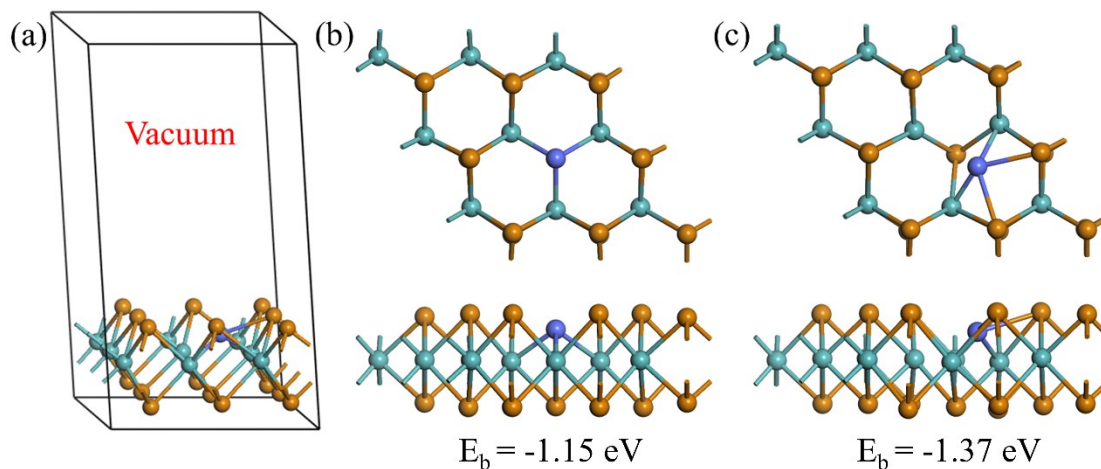$$E_b = -1.15 \text{ eV} \qquad E_b = -1.37 \text{ eV}$$

Figure S1. Schematic illustrations of the optimized structures. (a) 2H-MoTe$_2$ monolayer with a Te vacancy; (b) top-Co/MoTe$_2$;(c) center-Co/MoTe$_2$. Orange, cyan and blue balls refer to Te, Mo and Co atoms, respectively.
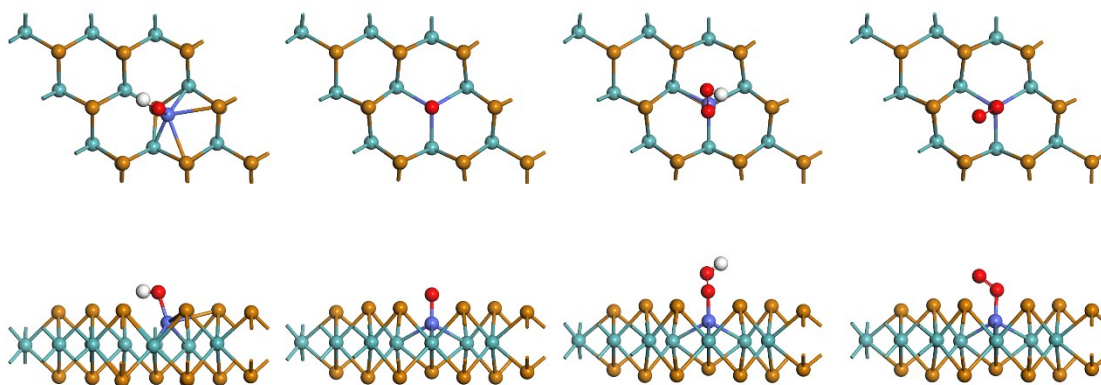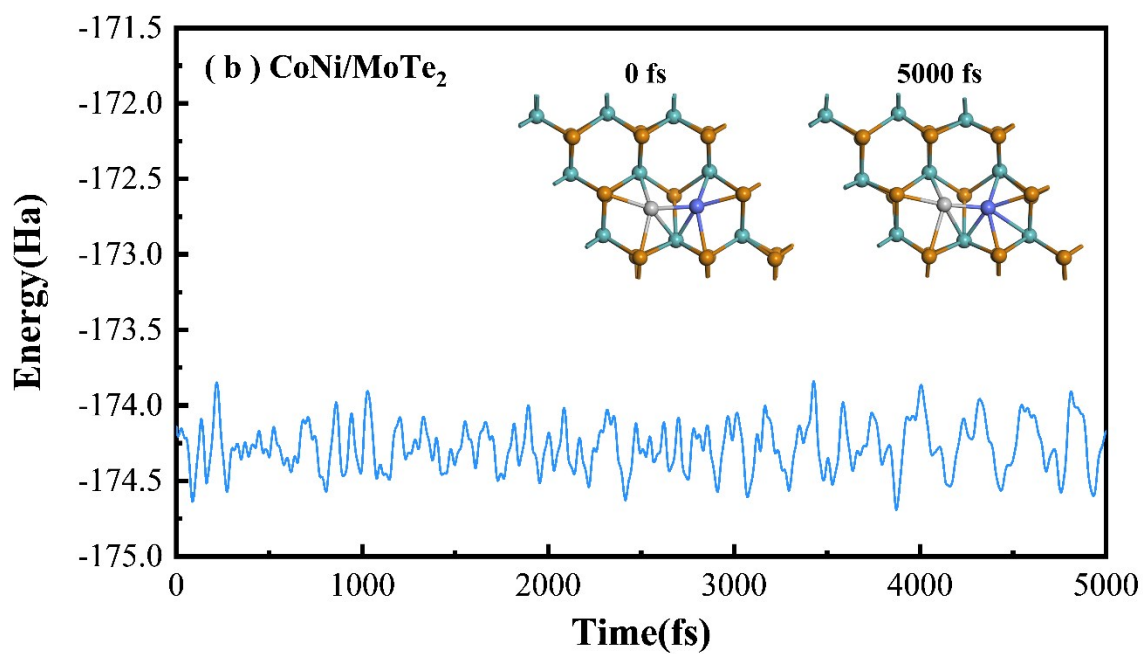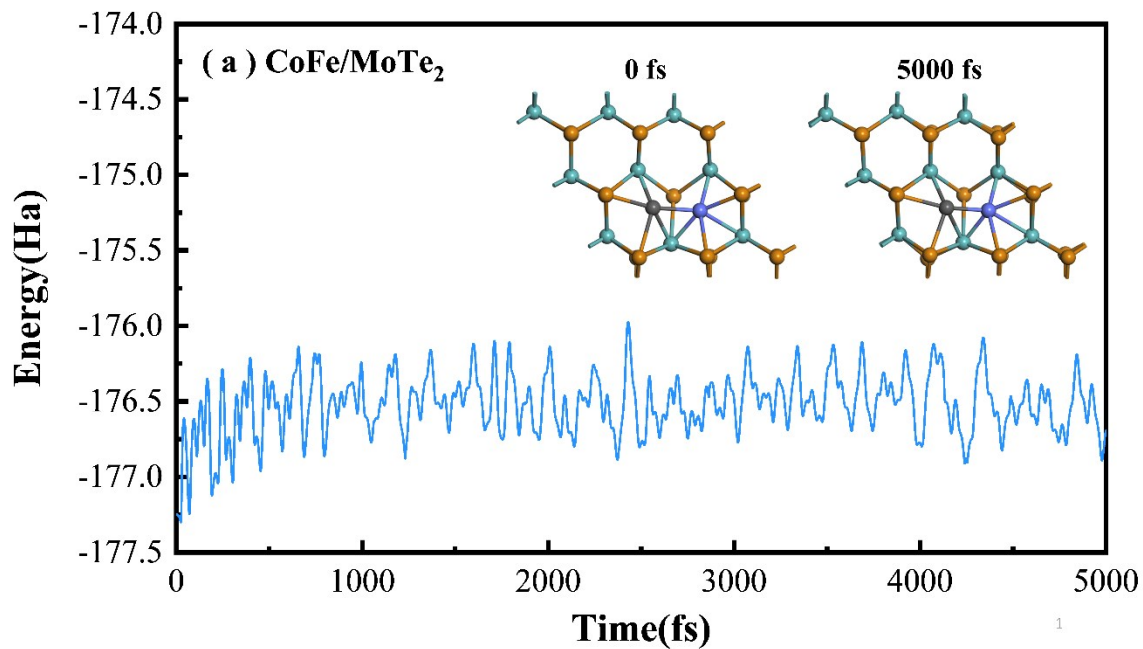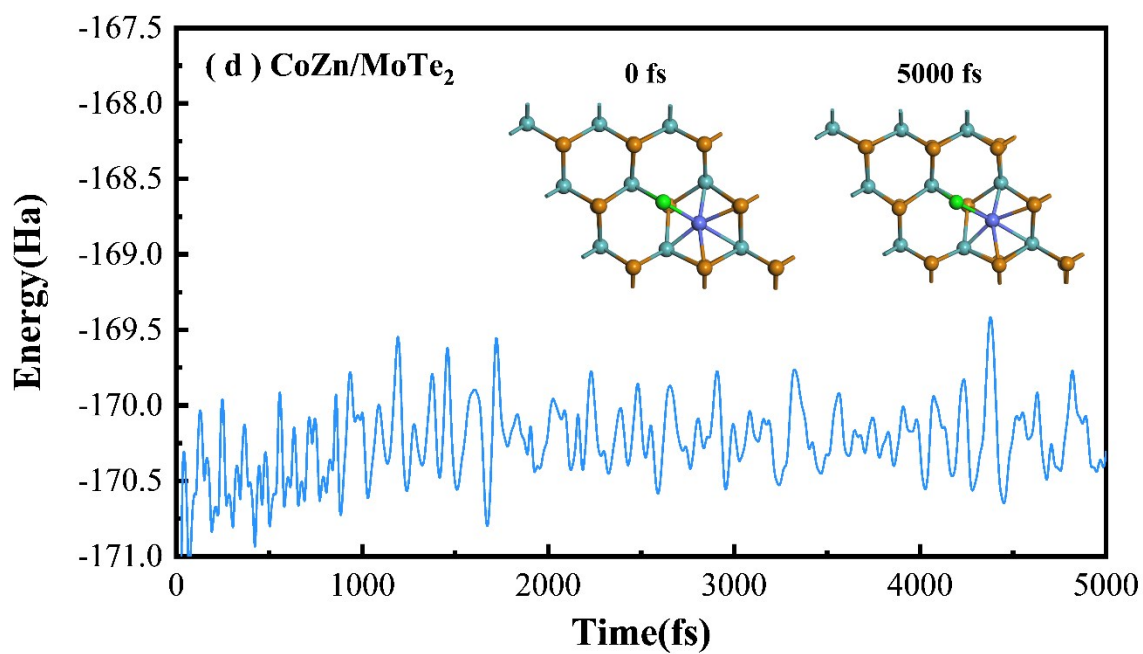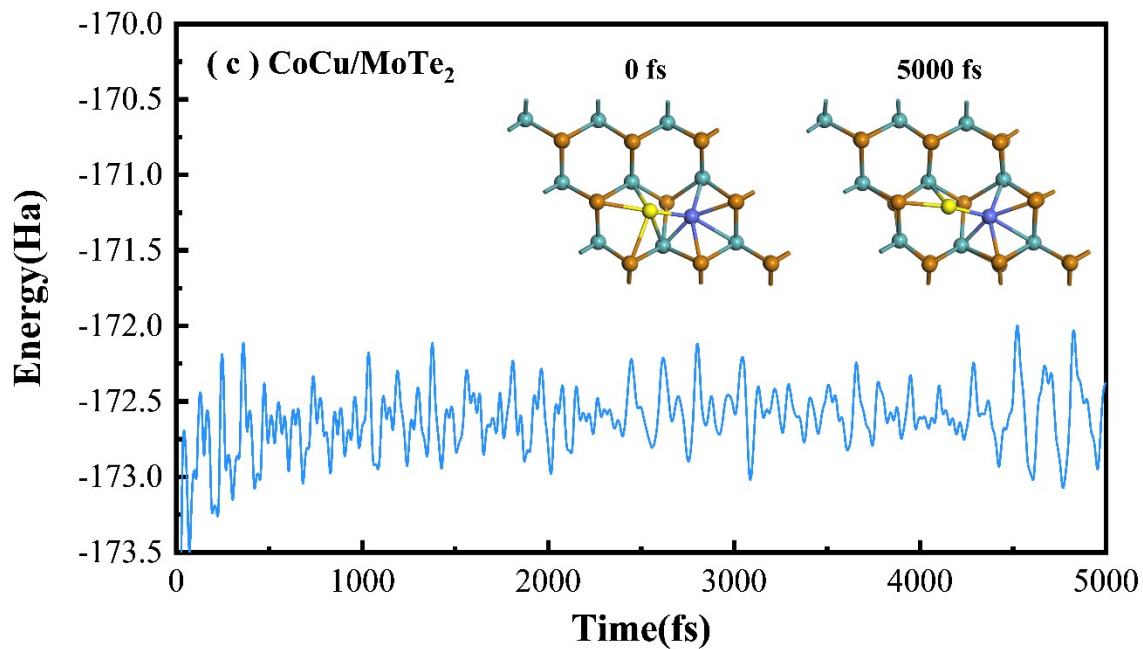

Figure S2. Optimized adsorption configurations for various OER/ORR species (including O$_2$, OOH, O, and OH) adsorbed on Co/MoTe$_2$ surface. Orange, cyan, blue, red and white balls refer to Te, Mo, Co, O and H atoms, respectively.
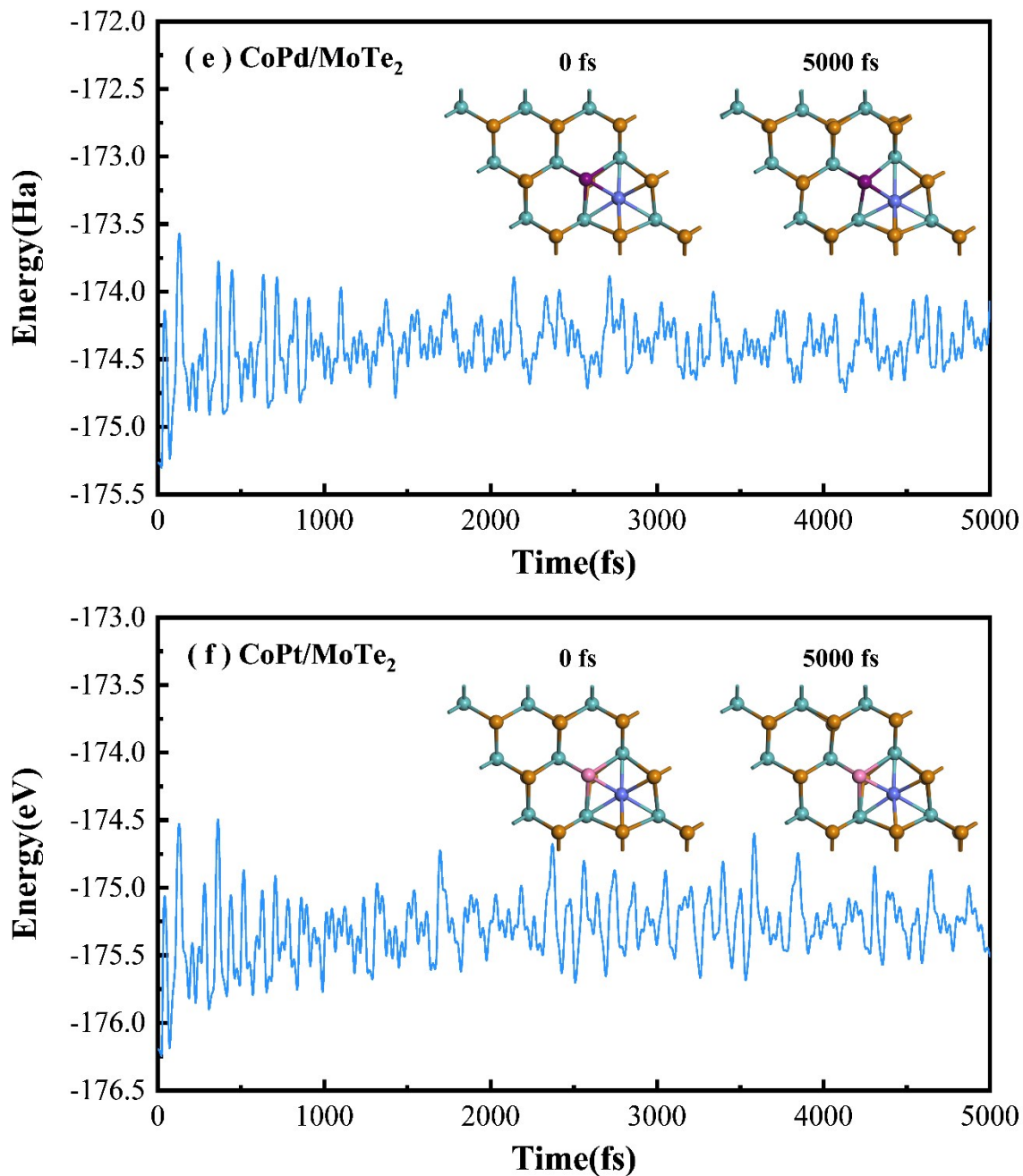
(c) CoCu/MoTe$_2$ 0 fs   5000 fs

(d) CoZn/MoTe$_2$ 0 fs   5000 fs

Figure S3. The energy equilibrium curves and corresponding snapshots for equilibrium structures of CoM/MoTe$_2$ at 500K using the simple Nosé-Hoover thermostat (a) CoFe/MoTe$_2$, (b) CoNi/MoTe$_2$, (c) CoCu/MoTe$_2$, (d) CoZn/MoTe$_2$, (e) CoPd/MoTe$_2$, (f) CoPd/MoTe$_2$
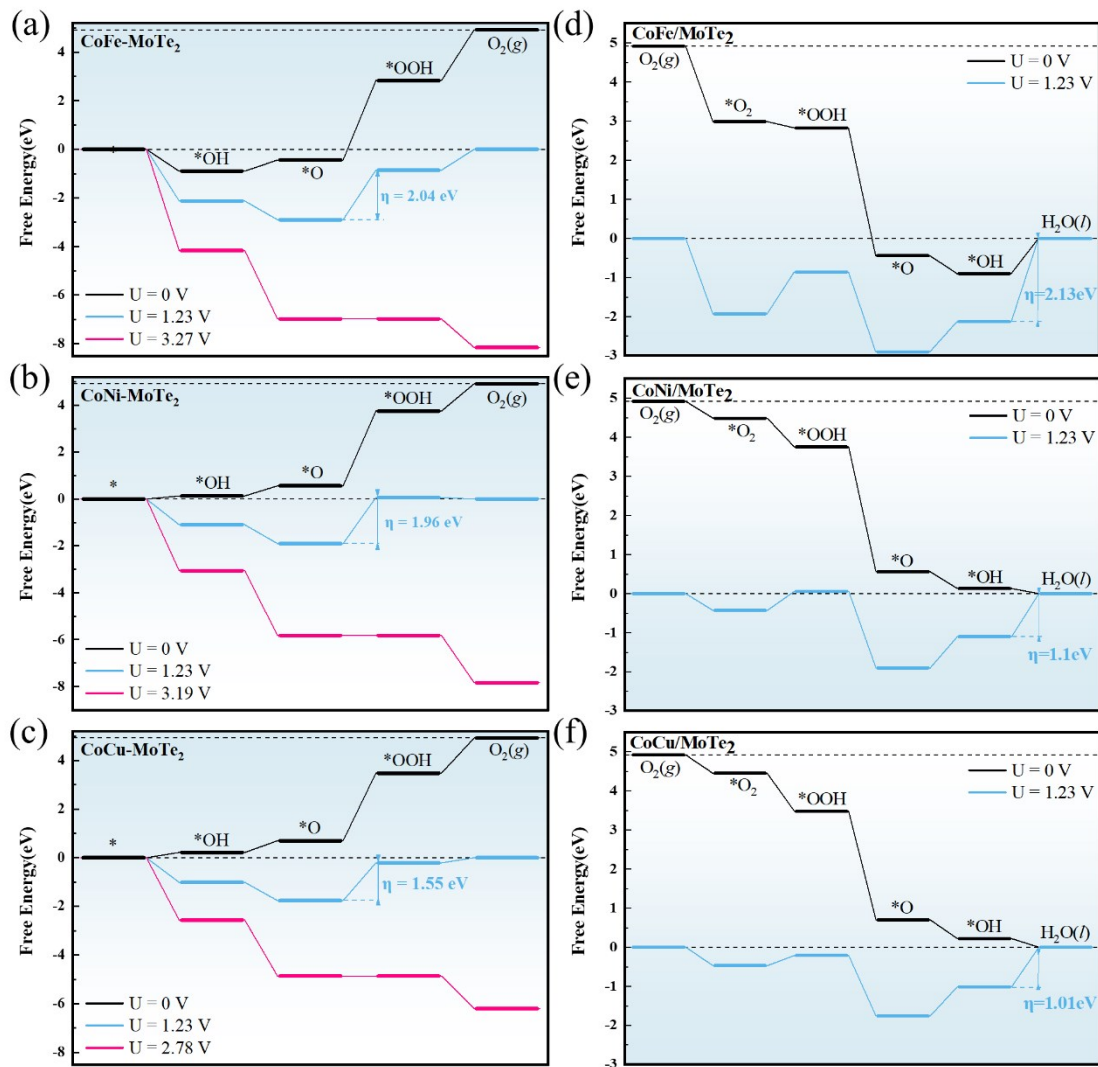
Figure S4. The free energy diagrams of the OER (a)(b)(c) and ORR (d)(e)(f) pathway for

CoZn/MoTe$_2$, CoPd/MoTe$_2$ and CoPt/MoTe$_2$.

0

Figure S5. Optimized adsorption configurations for various OER/ORR species (including O_2, OOH, O, and OH) adsorbed on CoFe/MoTe$_2$ surface. Orange, cyan, black, blue, red and white balls refer to Te, Mo, Fe, Co, O and H atoms, respectively.
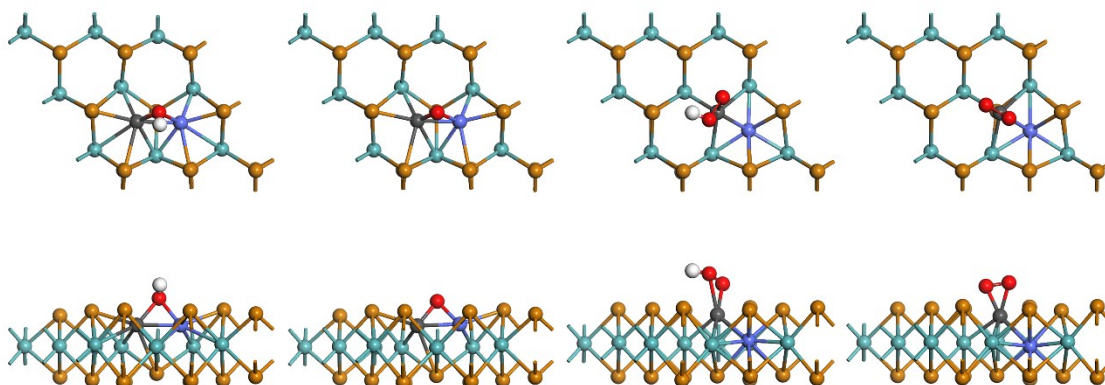

Figure S6. Optimized adsorption configurations for various OER/ORR species (including O_2, OOH, O, and OH) adsorbed on CoNi/MoTe$_2$ surface. Orange, cyan, silver, blue, red and white balls refer to Te, Mo, Ni, Co, O and H atoms, respectively.
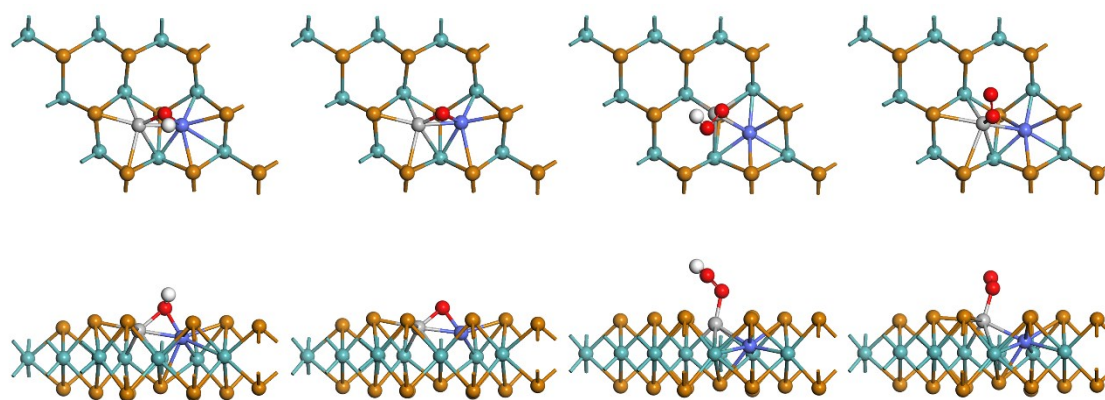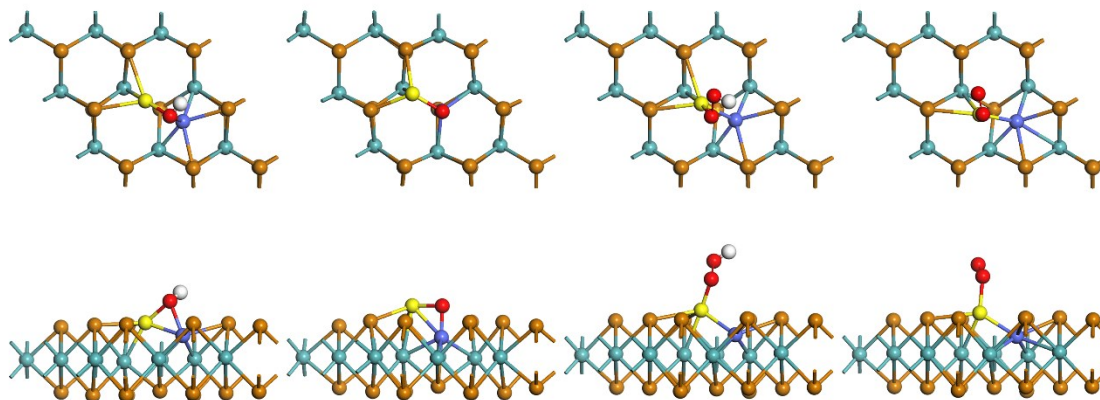
1

Figure S7. Optimized adsorption configurations for various OER/ORR species (including O$_2$, OOH, O, and OH) adsorbed on CoCu/MoTe$_2$ surface. Orange, cyan, yellow, blue, red and white balls refer to Te, Mo, Cu, Co, O and H atoms, respectively.

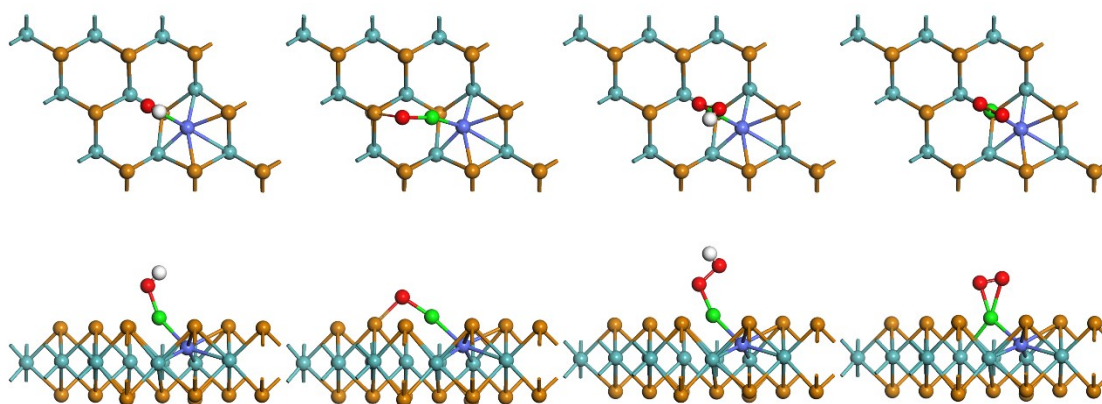**Figure S8.** Optimized adsorption configurations for various OER/ORR species (including O$_2$, OOH, O, and OH) adsorbed on CoZn/MoTe$_2$ surface. Orange, cyan, green, blue, red and white balls refer to Te, Mo, Zn, Co, O and H atoms, respectively.
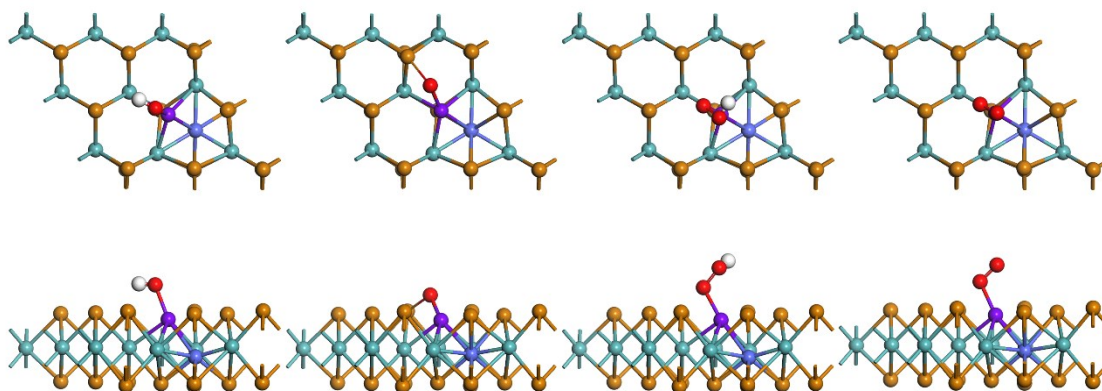
Figure S9. Optimized adsorption configurations for various OER/ORR species (including

O_2, OOH, O, and OH) adsorbed on CoPd/MoTe$_2$ surface. Orange, cyan, purple, blue,

red and white balls refer to Te, Mo, Pd, Co, O and H atoms, respectively.
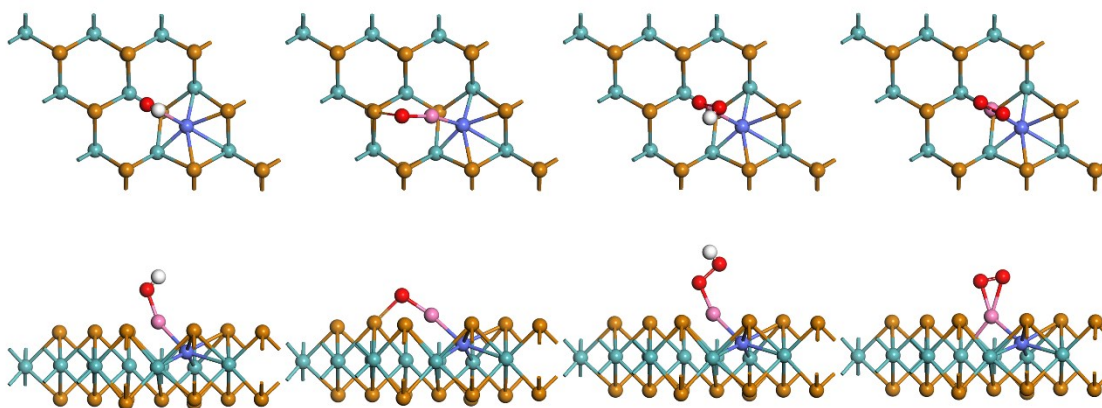

Figure S10. Optimized adsorption configurations for various OER/ORR species

(including O2, OOH, O, and OH) adsorbed on CoPt/MoTe$_2$ surface. Orange, cyan, pink,

blue, red and white balls refer to Te, Mo, Pt, Co, O and H atoms, respectively.
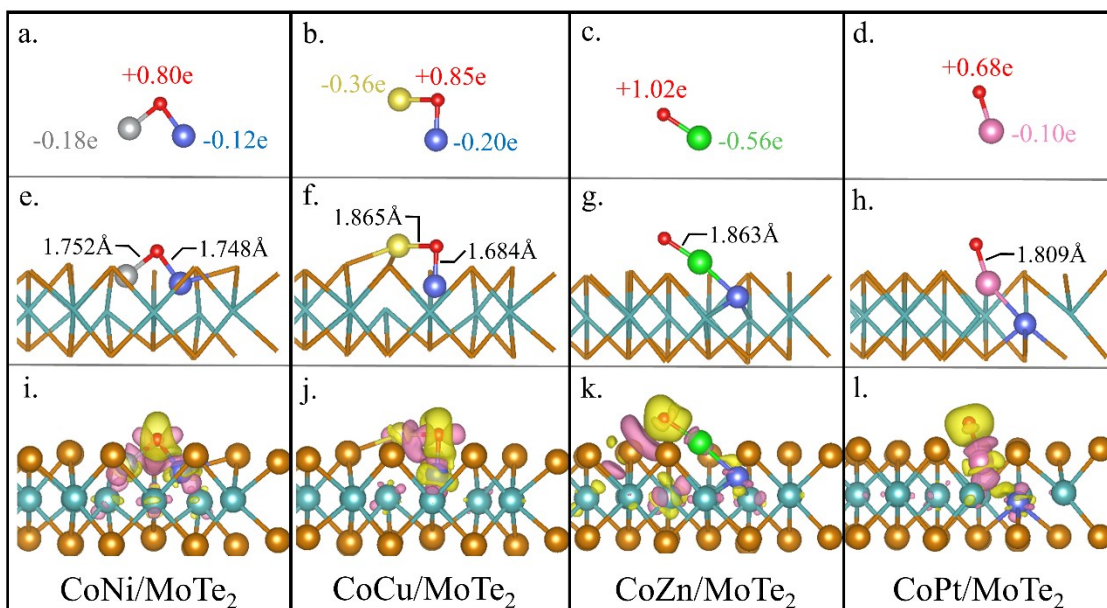
Figure S11. The schematic diagram of *O optimized configurations for different substrates. (i), (j), (k), (l): Side view of charge density difference of CoNi/MoTe$_2$, CoCu/MoTe$_2$, CoZn/MoTe$_2$, CoPt/MoTe$_2$ after adsorption of *O intermediates, respectively. The electron accumulation and depletion are described by the blue and pink regions with the isovalues of 0.005 eÅ^{-3}. (e), (f), (g), (h): the distribution of Bader effective charges; (a), (b), (c), (d): The bond length parameters. The orange, cyan, blue, silver, yellow, green, pink and red balls refer to Te, Mo, Co, Ni, Cu, Zn, Pt, and O atoms, respectively.

Table S1. Formation energies (E_f) of CoM/MoTe$_2$.

	E_f
CoFe-MoTe$_2$	-3.484
CoNi-MoTe$_2$	-1.498
CoCu-MoTe$_2$	-1.617
CoZn-MoTe$_2$	-1.835
CoPd-MoTe$_2$	-1.887
CoPt-MoTe$_2$	-1.858

Table S2. Reaction free energies (ΔG_{*ads}, eV) of the key OER intermediate species for doped MoTe$_2$.

	ΔG_1	ΔG_2	ΔG_3	ΔG_4
Co-MoTe$_2$	0.31	0.48	2.25	1.88
CoZn-MoTe$_2$	-0.09	1.69	1.72	1.60
CoPd-MoTe$_2$	0.59	1.39	1.87	1.07
CoPt-MoTe$_2$	0.23	1.17	2.06	1.46
CoFe-MoTe$_2$	-0.90	0.46	3.27	2.09
CoNi-MoTe$_2$	0.13	0.43	3.19	1.17
CoCu-MoTe$_2$	0.22	0.47	2.79	1.44

Table S3. Reaction free energies (ΔG_{*ads}, eV) of the key ORR intermediate species for doped $MoTe_2$.

	ΔG_0	ΔG_1	ΔG_2	ΔG_3	ΔG_4
Co-MoTe₂	-1.70	-1.18	-2.25	-0.48	0.69
CoZn-MoTe₂	-0.77	-0.84	-1.72	-1.69	0.09
CoPd-MoTe₂	-0.43	-0.65	-1.87	-1.39	-0.59
CoPt-MoTe₂	-0.58	-0.87	-2.06	-1.20	-0.20
CoFe-MoTe₂	-1.93	-0.16	-3.27	-0.46	0.90
CoNi-MoTe₂	-0.43	-0.75	-3.19	-0.43	-0.13
CoCu-MoTe₂	-0.47	-0.97	-2.79	-0.47	-0.22

Table S4. Spin moment (μ_B) of TM atoms in different substrates.

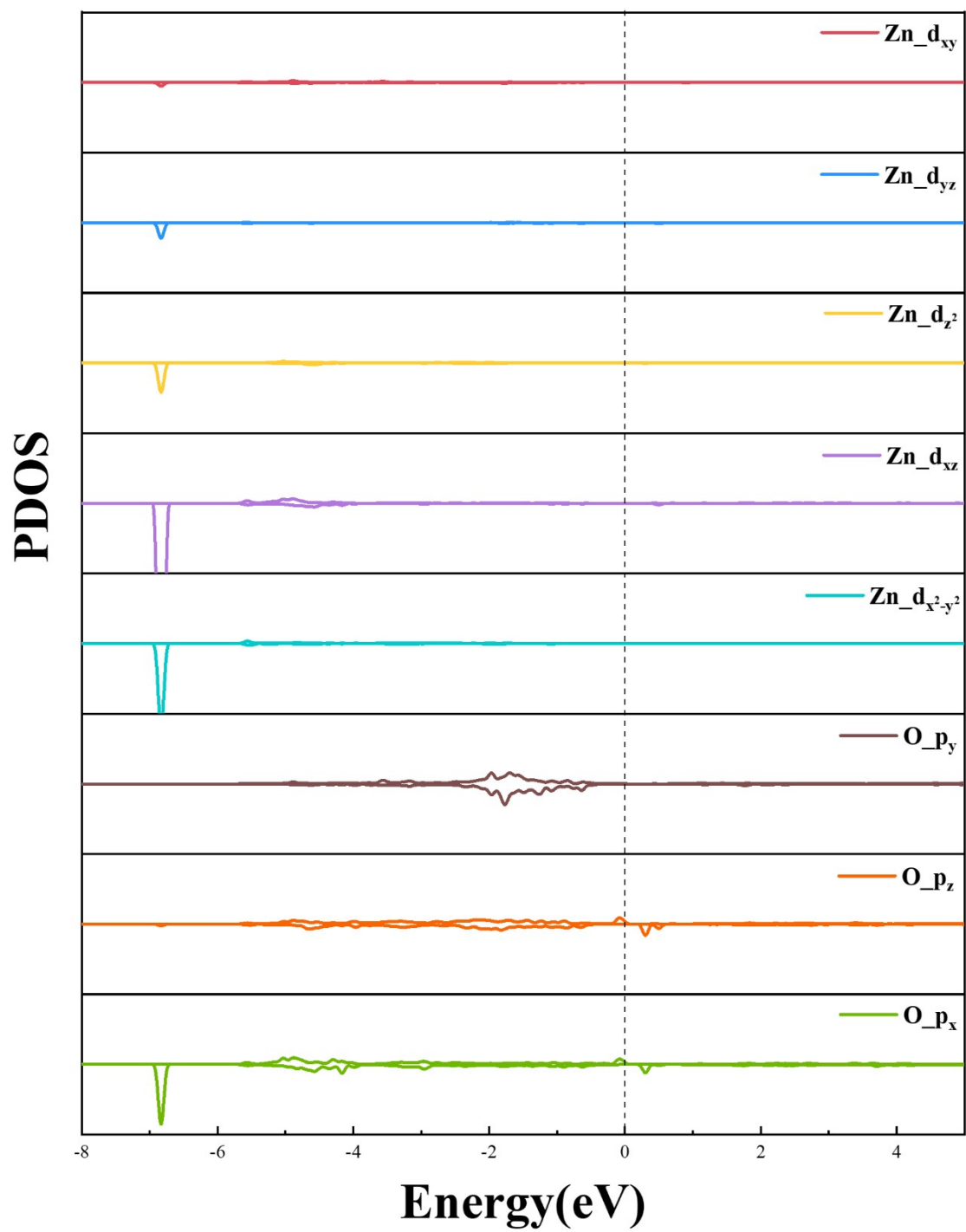|	Co	M
CoZn-MoTe₂	0.008	0.053
CoPd-MoTe₂	0.57	0.053
CoPt-MoTe₂	0.53	0.064
CoFe-MoTe₂	0.81	1.8
CoNi-MoTe₂	0.79	0.11
CoCu-MoTe₂	0	0

Figure S12. The PDOS of Zn atom in *O intermediate for CoZn/MoTe$_2$
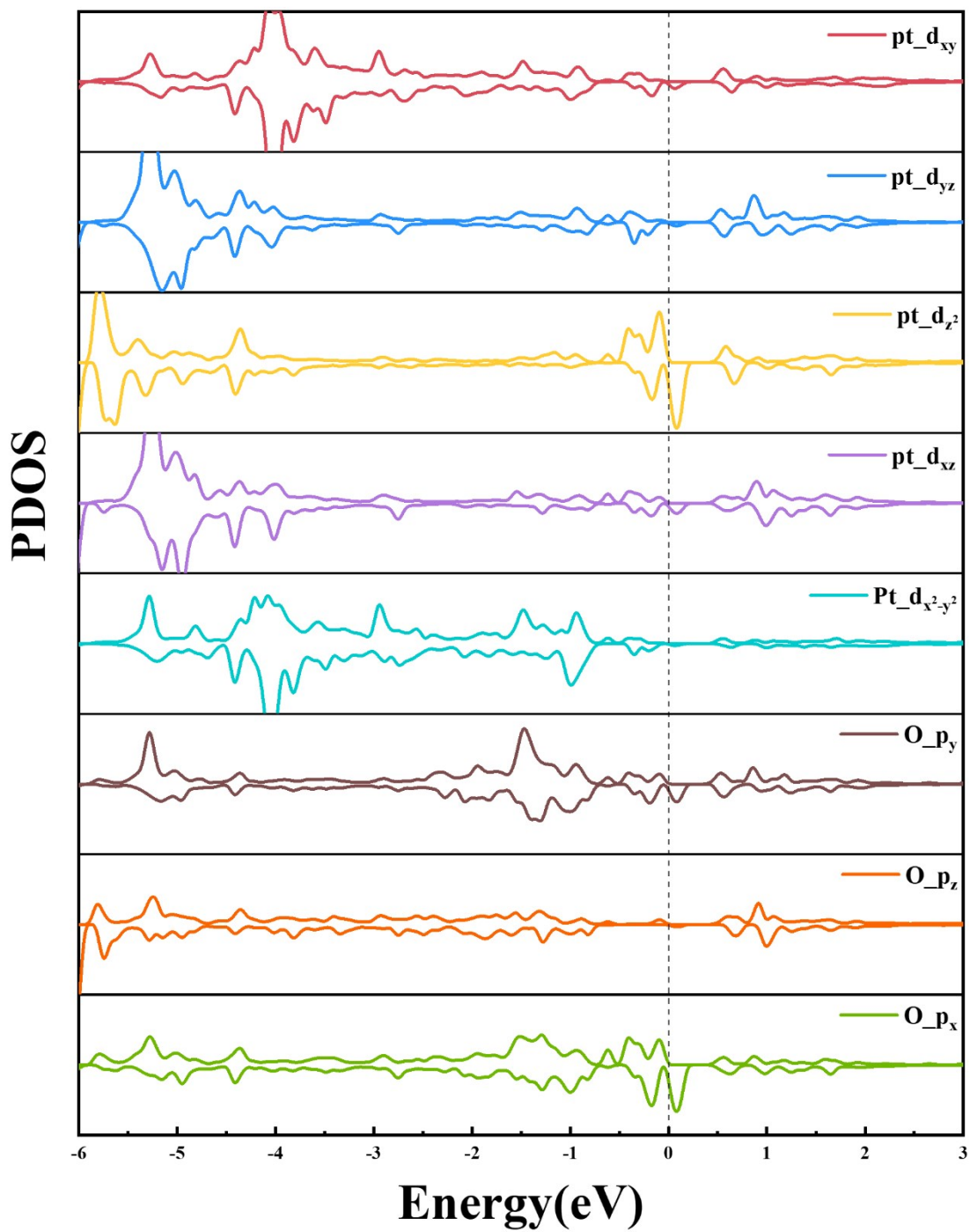
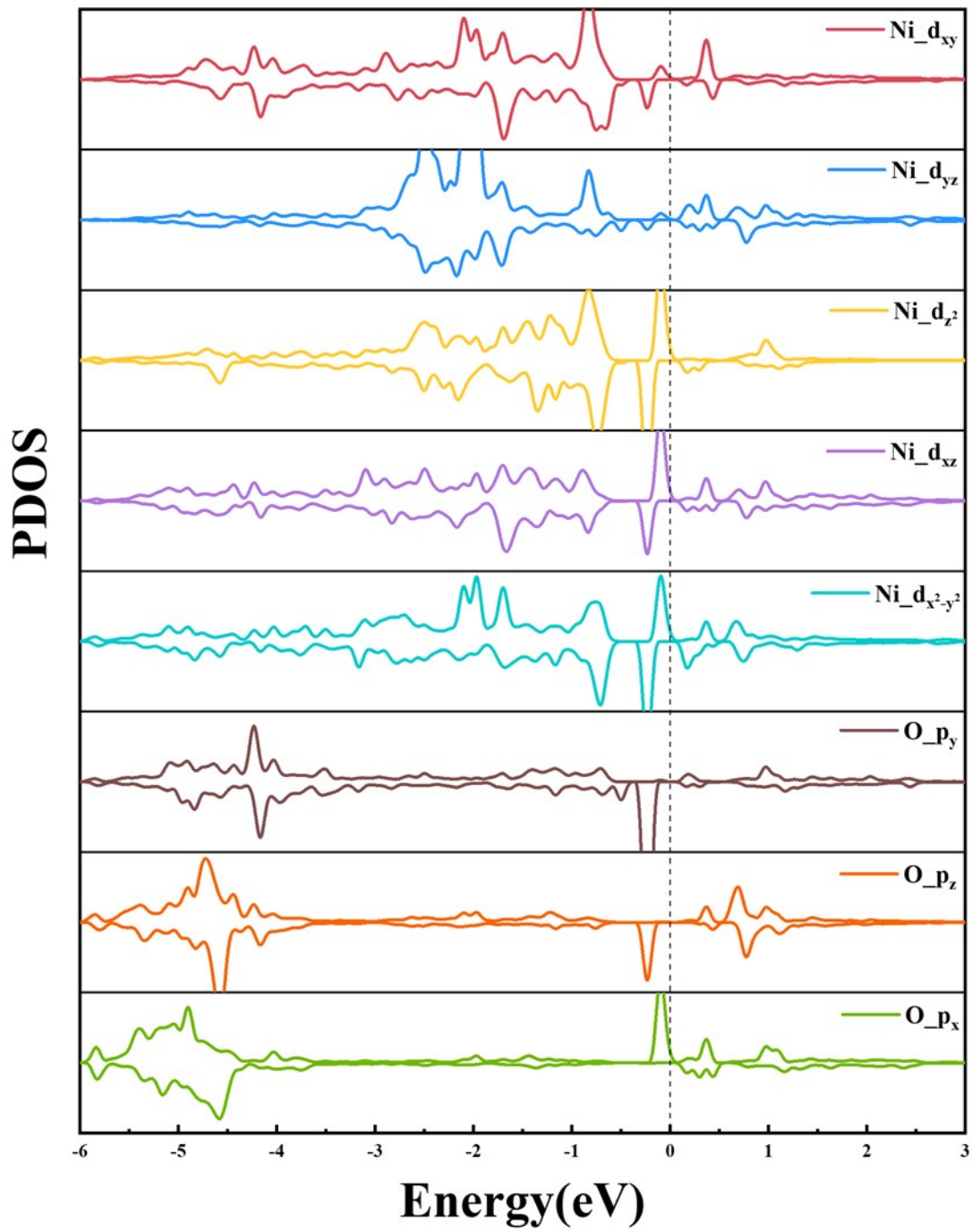**Figure S13.** The PDOS of Pt atom in *O intermediate for CoPt/MoTe$_2$

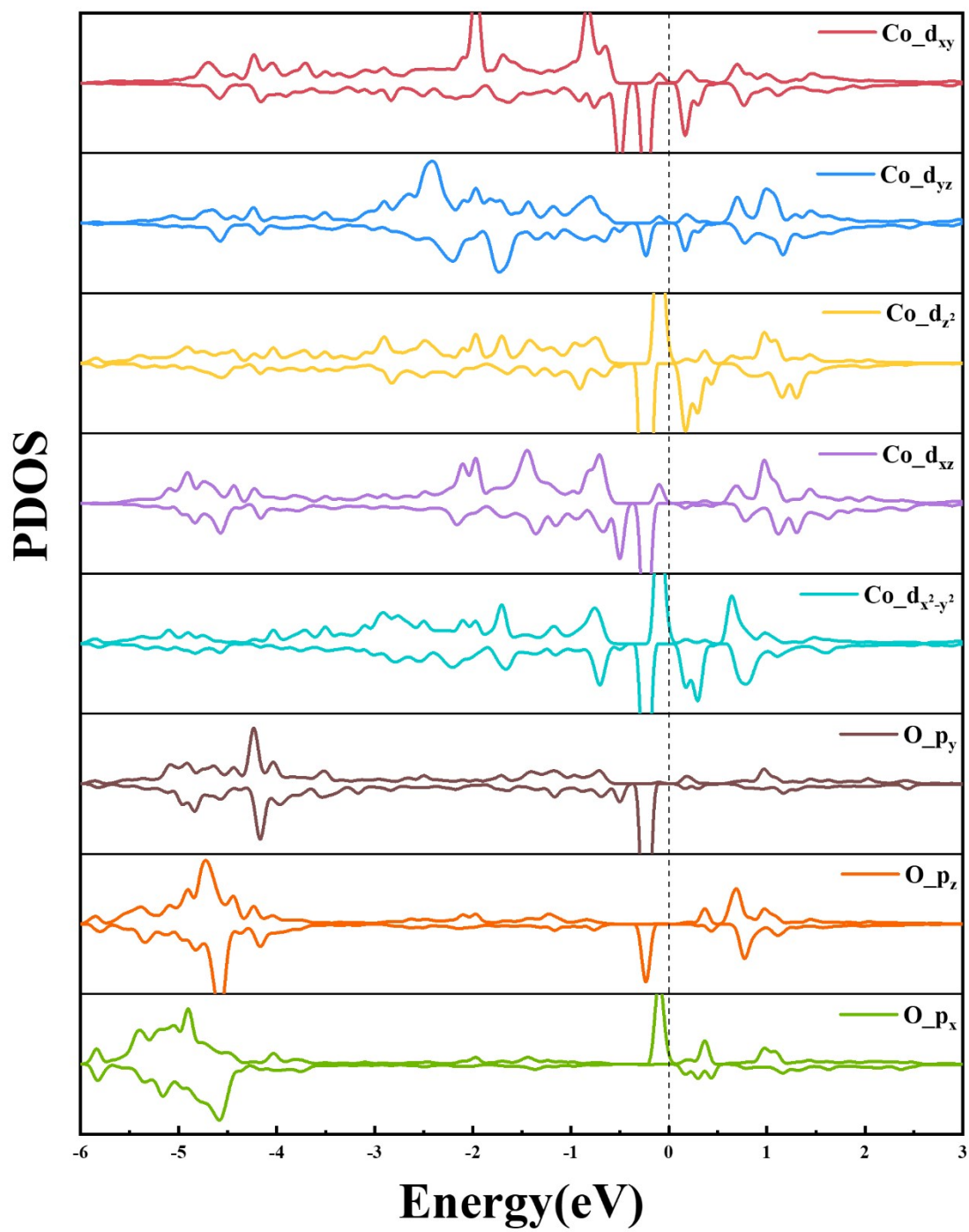**Figure S14.** The PDOS of Ni atom in *O intermediate for CoNi/MoTe$_2$

Figure S15. The PDOS of Co atom in *O intermediate for CoNi/MoTe$_2$

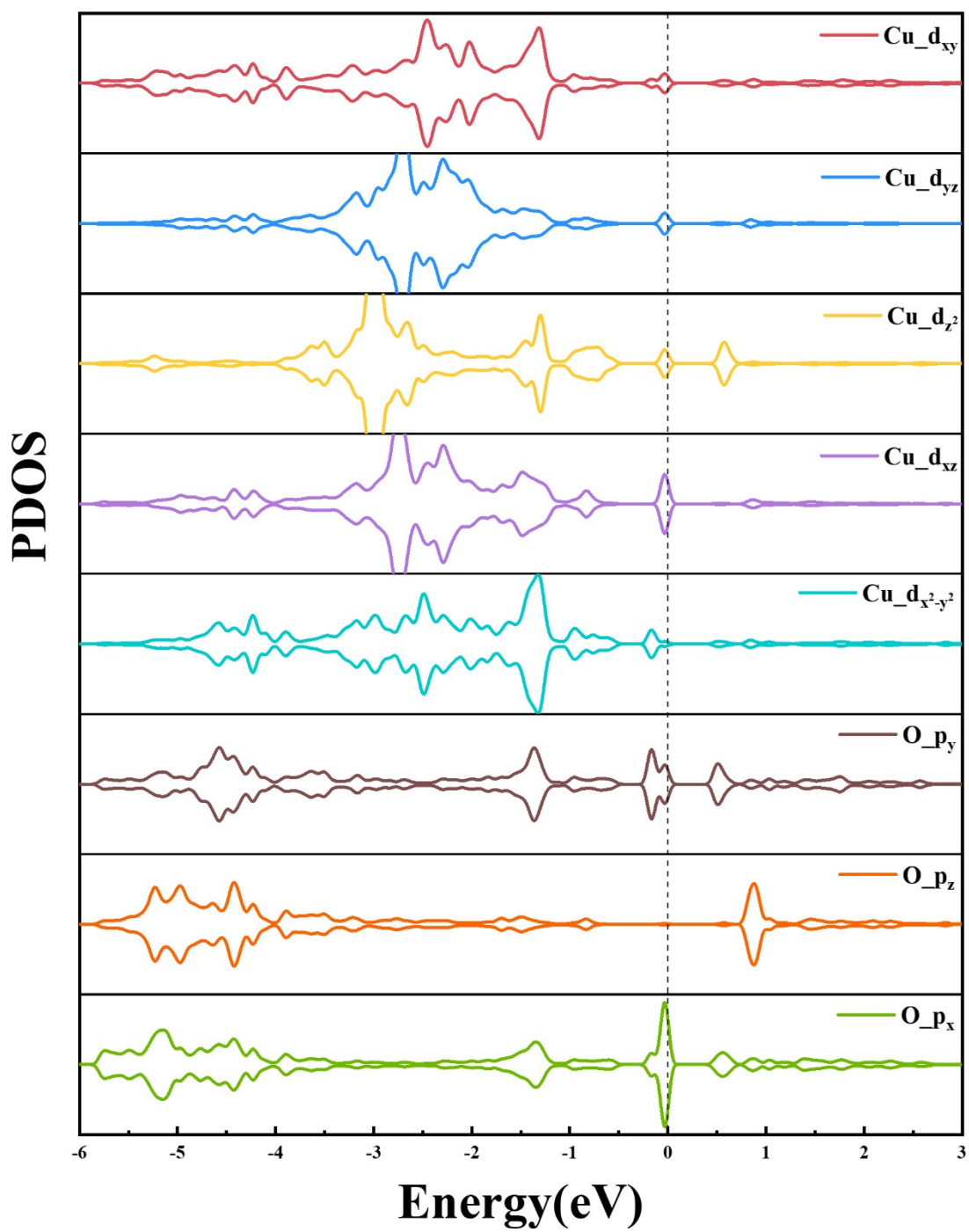**Figure S16.** The PDOS of Cu atom in *O intermediate for CoCu/MoTe$_2$
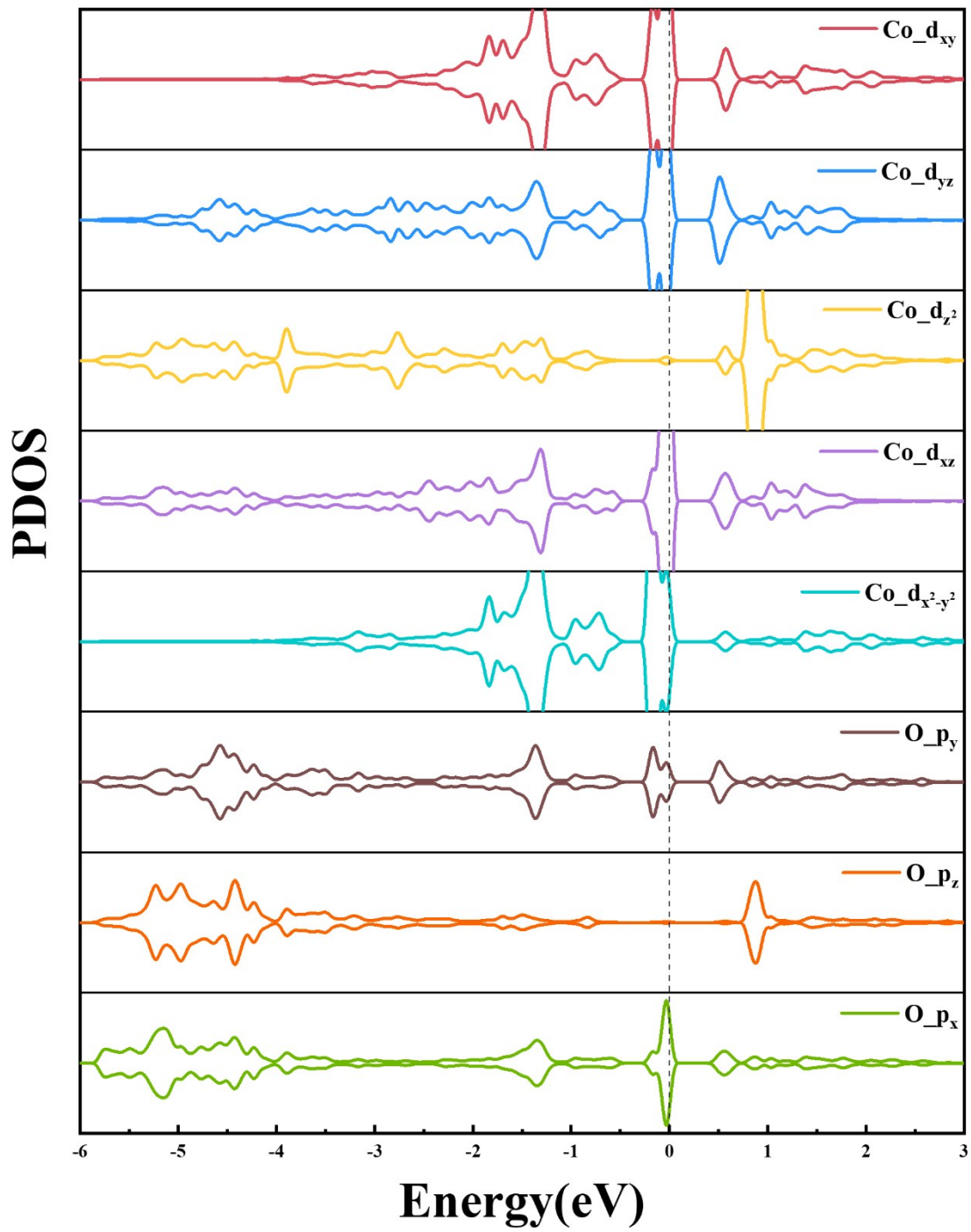
Figure S17. The PDOS of Co atom in *O intermediate for CoCu/MoTe$_2$

References

1. G. Kresse and J. Furthmüller, *Comp. Mater. Sci.*, 1996, **6**, 15-50.

2. G. Kresse and J. Furthmüller, *Phys. Rev. B.*, 1996, **4**, 11169-11186.

3. J. P. Perdew, J. A. Chevary, S. H. Vosko, K. A. Jackson, M. R. Pederson, D. J. Singh and C. Fiolhais, *Phys. Rev. B.*, 1992, **46**, 6671-6687.

4. J. P. Perdew, K. Burke and M. Ernzerhof, *Phys. Rev. Lett.*, 1996, **77**, 3865-3868.

5. S. Grimme, J. Antony, S. Ehrlich and H. Krieg, *J. Chem. Phys.*, 2010, **132**, 154104.

6. G. Kresse and D. Joubert, *Phys. Rev. B.*, 1999, **59**, 1758.

7. H. J. Monkhorst and J. D. Pack, *Phys. Rev. B.*, 1976, **13**, 5188-5192.

8. J. K. Nørskov, J. Rossmeisl, A. Logadottir, L. Lindqvist, J. R. Kitchin, T. Bligaard and H. Jónsson, *J. Phys. Chem. B.*, 2004, **108**, 17886-17892.

9. L. Seitz, C. Dickens, K. Nishio, Y. Hikita, J. Montoya, A. Doyle, C. Kirk, A. Vojvodic, H. Hwang, J. Norskov and T. Jaramillo, *Science*, 2016, **353**, 1011-1014.

10. J. Rossmeisl, Z. W. Qu, H. Zhu, G. J. Kroes and J. K. Nørskov, *J. Electroanal. Chem.,* 2007, **607**, 83-89.

11. I. C. Man, H.-Y. Su, F. Calle-Vallejo, H. A. Hansen, J. I. Martínez, N. G. Inoglu, J. Kitchin, T. F. Jaramillo, J. K. Nørskov and J. Rossmeisl, *Chem. Cat. Chem.*, 2011, **3**, 1159-1165.

4